Supplementary Information for

Decoupling chemical formation and vertical recirculation in driving urban ozone pollution

Zhenguo Liu[1], Yu Zou[2,*], Xin Song[1], Xiao-Bing Li[1,*], Bin Yuan[1], Chenglei Pei[3], Yuwen Peng[3], Jing Chen[1], Xuemei Wang[1], Min Shao[1]

[1] College of Environment and Climate, Institute for Environmental and Climate Research, Guangdong-Hongkong-Macau Joint Laboratory of Collaborative Innovation for Environmental Quality, Jinan University, Guangzhou, 511443, China

[2] Guangzhou Institute of Tropical and Marine Meteorology of China Meteorological Administration, GBA Academy of Meteorological Research, Guangzhou, 510640, China

[3] Guangzhou Sub-branch of Guangdong Ecological and Environmental Monitoring Center, Guangzhou, 510006, China

[*] Corresponding authors: Yu Zou (yzou@gd121.cn) and Xiao-Bing Li (lixiaobing@jnu.edu.cn)

This supplementary information document contains the following:

Text S1. Instruments.

Text S2. Source apportionment of the daily enhancement of column-integrated Ox in the PBL.

Text S3. Estimation of ozone and its precursor concentrations above the maximum measurement height on the Canton Tower.

Fig. S1 Distribution of the observation sites.

Fig. S2 Comparison of pollutant observations between GPMS and Canton Tower (surface) during the wet and dry seasons.

Fig. S3 Interannual variations of NO_2, O_3, and Ox at the PRD urban site in the dry and wet seasons.

Fig. S4 Mean values of meteorological parameters and air pollutant concentrations in the dry and wet seasons.

Fig. S5 Scatter plots of the typical VOCs species in the dry and wet seasons.

Fig. S6 Time series of ozone concentrations above the ground and surface net ozone production rates during typical ozone pollution episodes.

Fig. S7 Scatter plots of daily maximum ozone concentrations versus daily maximum $P_{net}(O_3)$ in the wet and dry seasons.

Fig. S8 Average diurnal variations in meteorological factors, trace gases, and VOCs in the dry and wet seasons.

Fig S9. Proportions of surface emissions, chemical formation, and residual layer contributions to Ox CIC during the enhanced observation period in the dry and wet seasons.

Table S1 The minimum detection limit (MDL) for each VOCs species.

Text S1. Instruments

In this study, ozone was measured using the ultraviolet photometry method (49i, Thermo Fisher Scientific Inc., USA). NOx was measured using the chemiluminescence method (42i, Thermo Fisher Scientific Inc., USA). The national environmental monitoring site reported atmospheric pollutant mass concentrations under conditions of 273.15 K and 1013.25 hPa prior to 2019, and under conditions of 298.15 K and 1013.25 hPa after 2019. Here, we convert the mass concentrations of O_3 and NO_2 (μg m^{-3}) to volume mixing ratios (ppbv) to eliminate the impact of these variations on trend calculations.

Volatile organic compounds (VOCs, including NMHCs and OVOCs) were continuously measured using an online GC-MS/FID system (TH-300B, Wuhan Tianhong Environmental Protection Industry Co., Ltd.). Ambient air samples were automatically collected and delivered to the preconcentration module, where they were divided into two independent analytical pathways for targeted VOC separation and detection. In the FID channel, water vapor and CO_2 were removed from ambient air through temperature reduction and material adsorption, respectively. The C2–C5 hydrocarbon components were subsequently trapped on a PLOT capillary column at -150 °C. In parallel, the MS channel first removed water vapor at -150 °C, followed by the enrichment of C5–C12 hydrocarbons and OVOCs using a dedicated capillary column. After pre-concentration, the trapping columns were rapidly heated, and the enriched VOCs were purged into the GC system by carrier gas for subsequent separation and detection. Specifically, C2–C5 hydrocarbons were separated by the PLOT column and quantified via the FID detector, whereas C5–C12 hydrocarbons and OVOCs were separated using a DB-624 capillary column and identified and quantified by the MS detector.

Different qualitative and quantitative strategies were adopted for the two detection channels. The FID-based quantification relied on retention time matching and the external standard method, while MS detection achieved compound identification through combined retention time and mass spectral matching with standard references, coupled with the internal standard method for quantification. Strict instrument calibration and quality control were implemented throughout the observation period.

Weekly single-point calibration and monthly five-point calibration were performed routinely using US-EPA certified mixed standard gas (PAMs+TO15, Linde) and a four-component internal standard gas mixture (bromochloromethane, 1,4-difluorobenzene, chlorobenzene-d5, and 4-bromofluorobenzene, Linde). The linear correlation coefficients for all target VOCs ranged from 0.98 to 0.99.

Text S2. Source apportionment of the daily enhancement of column-integrated Ox in the PBL

Following Song et al. (2024), Ox rather than O_3 is apportioned. The CIC of Ox in a given air layer is calculated with Eq. (1) of the main text. The enhancement of $CIC_{PBL}(Ox)$ relative to its nocturnal mean over 03:00–05:00 LT, an interval in which air masses vary little under the stable conditions that prevailed during the episodes, is attributed to three processes, namely the downward entrainment of Ox from the nocturnal residual layer, net chemical formation and surface emission:

$$\Delta CIC_{PBL}(Ox)_t = C_{RL}(Ox)_t + C_E(Ox)_t + C_{CF}(Ox)_t \quad \text{(S1)}$$

The residual-layer term is the Ox left above the boundary layer when it contracted at sunset, minus the Ox that remains above it at time t. For brevity, $CIC_X(a\rightarrow b)\ t$ denotes the CIC of species X between heights a and b at time t, evaluated with Eq. (1):

$$C_{RL}(Ox)_t = CIC_{Ox}(BLH_{night} \rightarrow RLH_{night})_{night} - CIC_{Ox}(BLH_t \rightarrow RLH_t)_t \quad \text{(S2)}$$

where *BLH* and *RLH* are the heights of the boundary layer and of the residual layer, the latter taken as the top reached by the daytime boundary layer on the preceding day.

The emission term is the Ox contributed by primary NO_2 emissions, estimated from the increase in the NOx burden over the same interval:

$$C_E(Ox)_t = (CIC_{NOx}(0 \rightarrow RLH_t)_t - CIC_{NOx}(0 \rightarrow RLH_{night})_{night}) \times ER \quad \text{(S3)}$$

where *ER* is the primary NO_2 to NOx emission ratio of combustion sources, set to 10% (Song et al., 2024). Only directly emitted NO_2 contributes to Ox, because the conversion of NO to NO_2 by O_3 conserves Ox. The chemical term follows as the remainder, $C_{CF}(Ox)_t = \Delta CIC_{PBL}(Ox)_t - C_E(Ox)_t$, so the three terms close on the observed enhancement.

Concentrations between two inlet heights are obtained by linear interpolation, and the value at the lowest inlet is used below it. Above 488 m they are prescribed as described in Text S3. NOx in Eq. (S3) is represented by NO_2, the only nitrogen oxide measured on the tower, which slightly underestimates the emission term. The residual layer is taken as horizontally homogeneous and its composition as time-invariant

between the reference interval and morning entrainment. No term represents horizontal advection, so the residual-layer term is a net quantity that also includes Ox transported into the region. The chemical term is obtained as the remainder.

Text S3. Estimation of ozone and its precursor concentrations above the maximum measurement height on the Canton Tower

The nocturnal boundary layer height usually falls below the elevation of Canton Tower's observations at 488 m. Observations at this height can represent the true state of the residual layer. Following Method III of Song et al. (2024), the concentrations of O3 and NO2 above 488 m were set equal to their mean values measured at 488 m between 00:00 and 06:00 LT of the same night.

The method was applied only on nights when the nocturnal boundary layer remained below 488 m. Days on which it rose above 488 m were excluded, since the inlet would otherwise lie within the boundary layer rather than the residual layer. It assumes that pollutant concentrations within the residual layer exhibit no significant vertical gradients and do not change substantially over time from nighttime through the early morning hours. Our previous studies have confirmed that this method shows good consistency with the trends of boundary layer trace gas column concentrations derived from satellite inversions (Song et al., 2024). Potential vertical gradients between the 118 m and 488 m levels during stable nocturnal conditions may introduce uncertainty that the available measurements cannot resolve, so no correction is applied for this gradient. The good agreement with satellite-derived column concentrations nevertheless supports the applicability of this approach for quantifying PBL-integrated pollutant burdens.

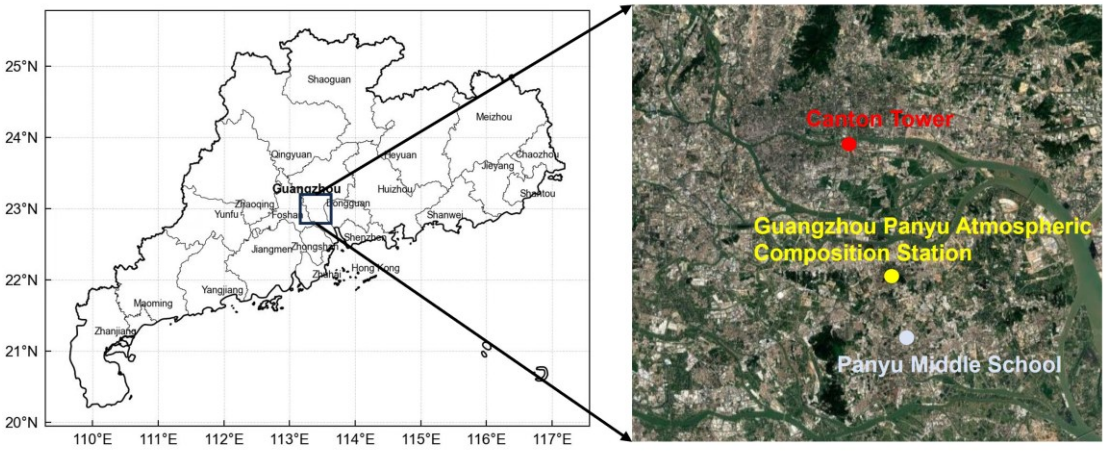


Fig. S1 Distribution of the observation sites. Map data in the right panel: © Google Earth 2026.

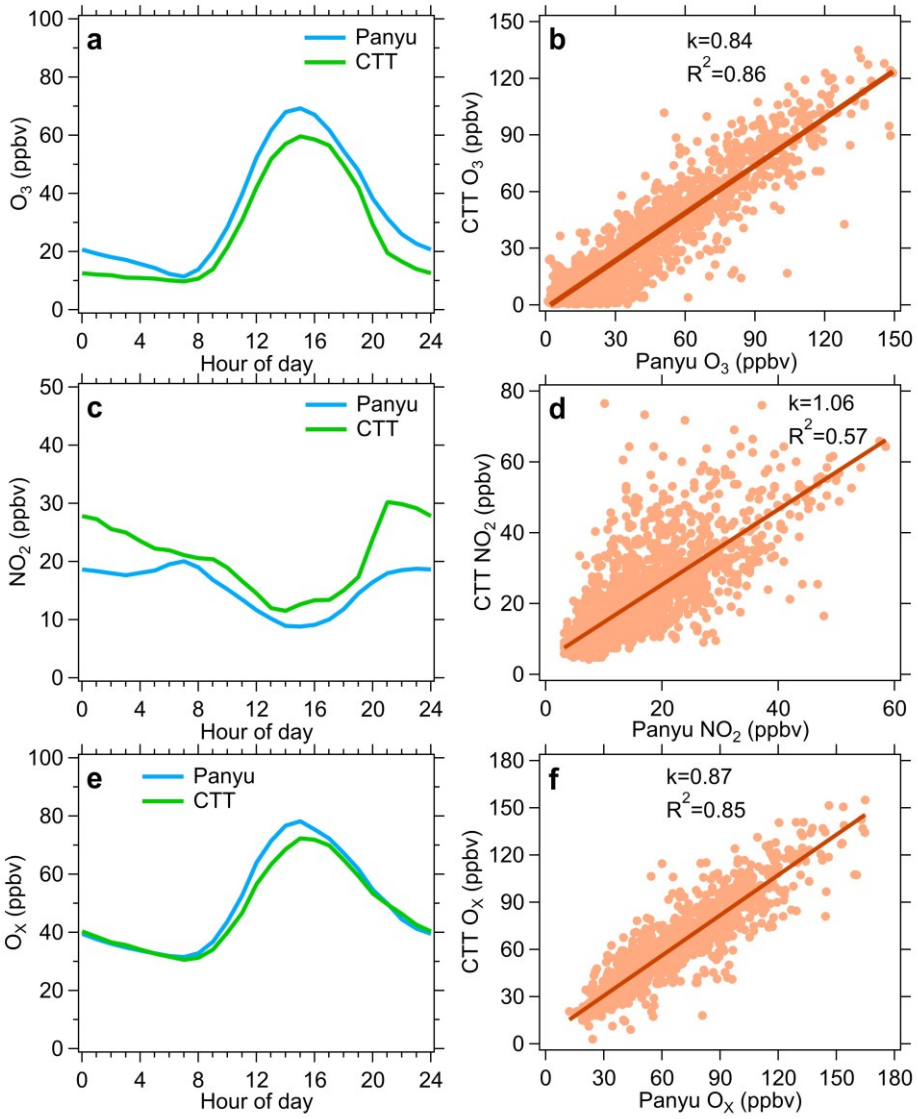


Fig. S2 Comparison of pollutant observations between the Guangzhou Panyu Middle School (GPMS) and Canton Tower (CTT, surface) sites during the wet (July–August 2024) and dry (March 2025) seasons. a, c, e, Average diurnal variations of O_3, NO_2, and Ox. b, d, f, Scatter plots of hourly concentrations with linear regression.

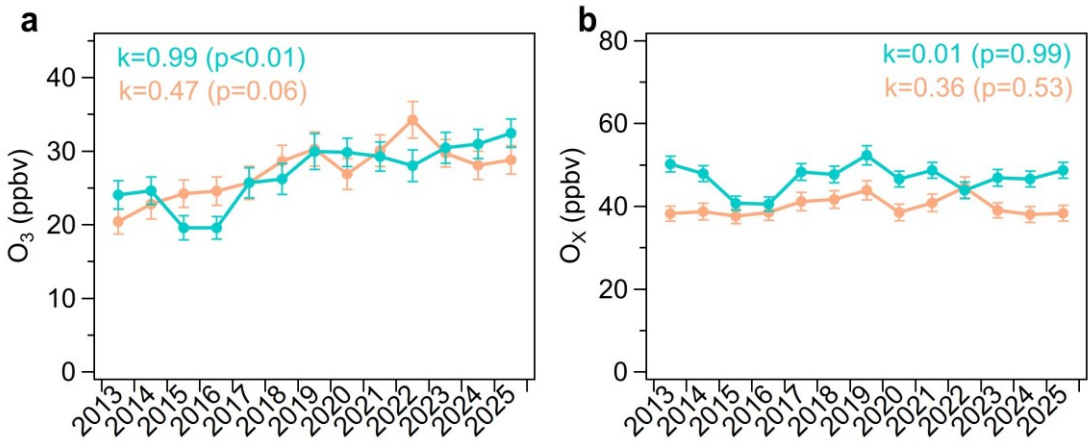


Fig. S3 Interannual variations of O_3 (a) and Ox (b) at the PRD urban site in the dry and wet seasons. Error bars show ±10% standard deviation (s.d.). The values of *k* represent the long-term trends of surface O_3 and Ox from 2015 to 2025.The study covers eight representative urban observation sites in the PRD region: Luhu (Guangzhou), Jinjuzui (Foshan), Zimaling (Zhongshan), Huijingcheng (Foshan), Chengzhong (Zhaoqing), Tangjia (Zhuhai), Donghu (Jiangmen), and Xiapu (Huizhou).

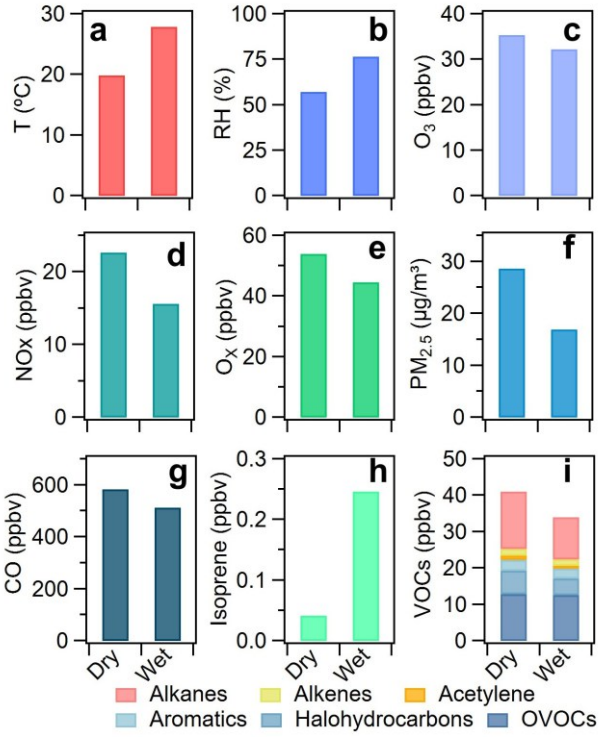


Fig. S4 Mean values of meteorological parameters and air pollutant concentrations in the dry and wet seasons.

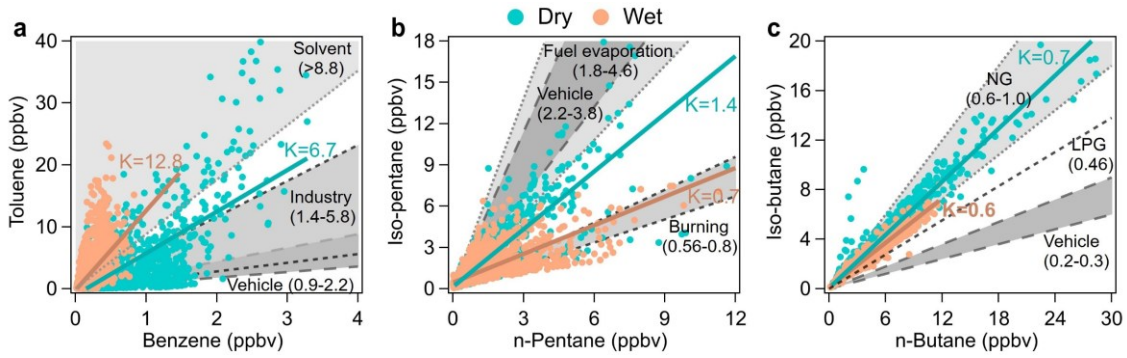


Fig. S5 Scatter plots of the typical VOCs species in the dry and wet seasons. a, Toluene *v.s.* Benzene. **b,** Iso-pentane *v.s.* n-Pentane. **c,** Iso-butane *v.s.* n-Butane. Solid lines indicate linear fitting lines.

This study used the specific species ratio to identify seasonal changes in the primary sources of AVOCs in the PRD. The results for the toluene/benzene (T/B) ratio show that the fitted slope during the wet season was 12.8, falling within the characteristic range for solvent usage (>8.8)(Zheng et al., 2013; Yuan et al., 2010). This may be related to the accelerated volatilization of chemicals such as paints and industrial solvents due to high temperatures. During the dry season, the slope decreased to 6.7, falling between the characteristic ranges for industrial sources (1.4–5.8) (Mo et al., 2015; Shi et al., 2015) and solvent usage (>8.8) (Song et al., 2021), suggesting a mixed contribution from these two source categories. Although there was some deviation in the characteristic ratios between the wet and dry seasons, the overall distribution of data points remained concentrated within the characteristic ranges of typical anthropogenic emissions, with no fundamental shift across emission categories. During the dry season, iso-pentane/n-pentane ratio was 1.4, reflecting the combined contribution of vehicle exhaust (2.2–3.8) and fuel evaporation (1.8–4.6)(Li et al., 2019). It dropped to 0.7 during the wet season, indicating a relative increase in the contribution from burning-related emissions (0.56-0.8)(Yan et al., 2017). Furthermore, the iso-butane/n-butane ratio remained consistently within the characteristic range for natural gas leaks (0.6–1.0)(Barletta et al., 2002; Russo et al., 2010) during both the dry and wet seasons, showing no significant seasonal variation. Overall, the variations in the ratios of these typical signature species between the dry and wet seasons reflect only minor fluctuations in the relative contributions of different sectors within anthropogenic sources, rather than fundamental changes in the overall structure of emission sources.

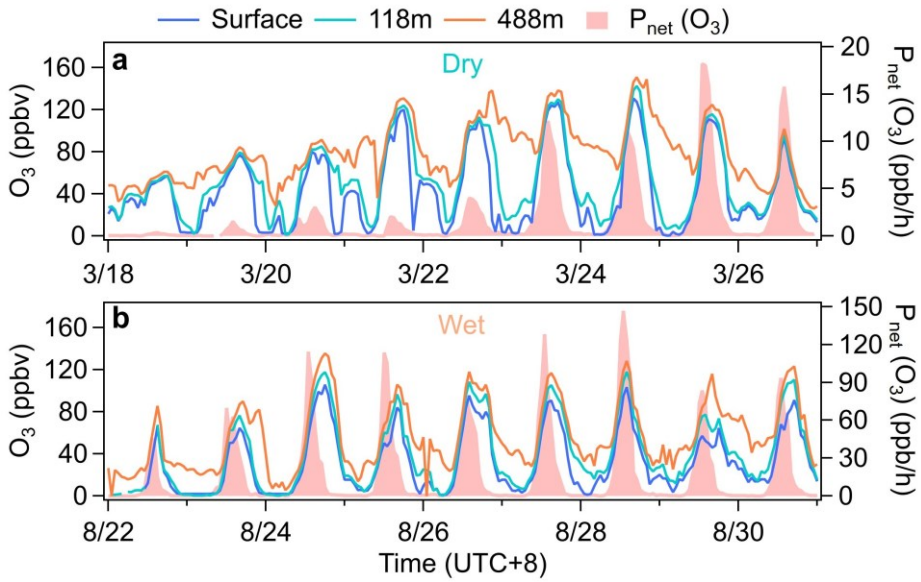


Fig. S6 Time series of ozone concentrations above the ground and surface net ozone production rates during typical ozone pollution episodes. a, The dry season**. b,** The wet season**.**

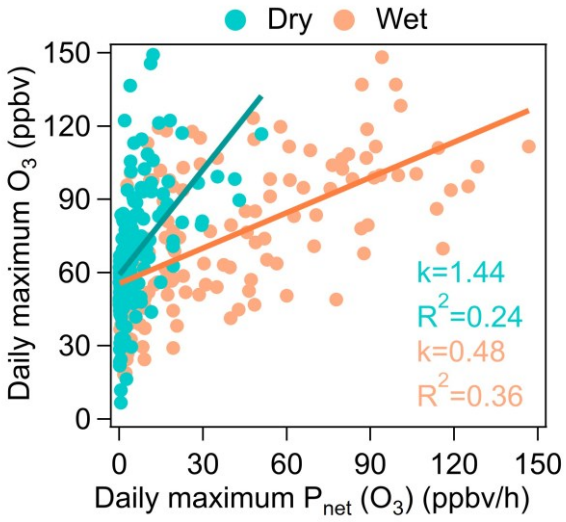


Fig. S7 Scatter plots of daily maximum ozone concentrations versus daily maximum $P_{net}(O_3)$ in the wet and dry seasons. Solid lines indicate linear fitting lines.

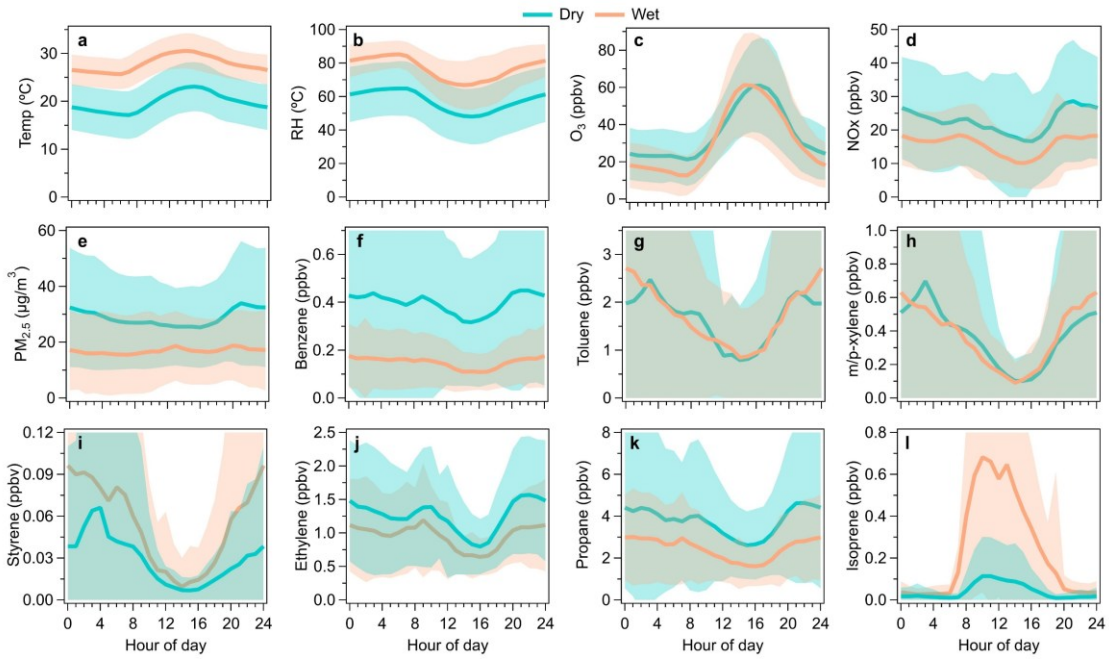


Fig. S8 Average diurnal variations in meteorological factors, trace gases, and VOCs in the dry and wet seasons.

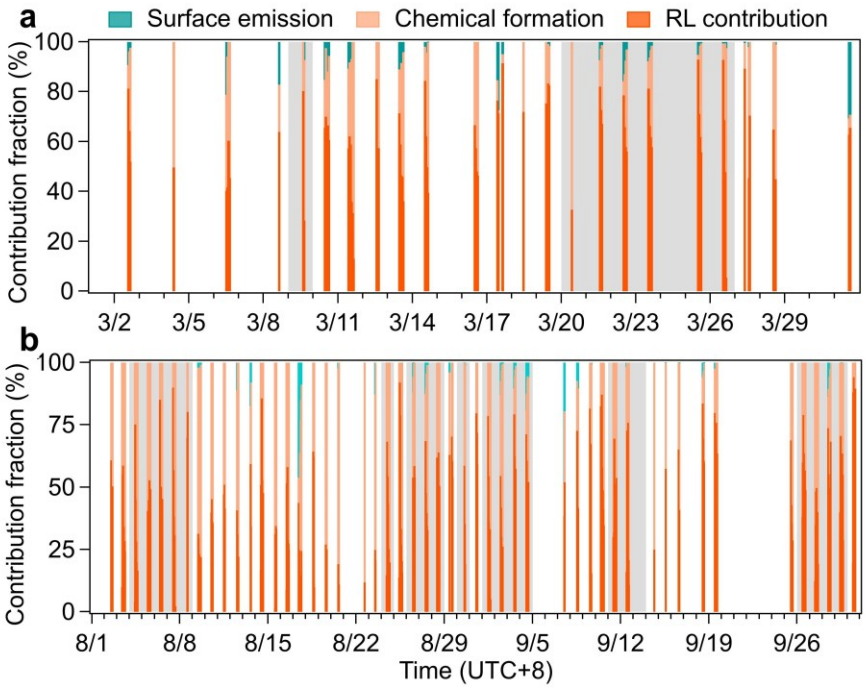


Fig S9. Proportions of surface emissions, chemical formation, and residual layer contributions to Ox CIC during the enhanced observation period in the dry and wet seasons. The data cover the 08:00–14:00 time window on daily basis during March 2025 and August–September 2024, with days exceeding the standard shaded.

Table S1 The minimum detection limit (MDL) for each VOCs species.

Species	MDL	Species	MDL	Species	MDL
Ethane	0.043	trans-1,2-Dichloroethene	0.037	cis-1,3-Dichloropropene	0.017
Ethylene	0.046	1-Hexene	0.027	1,1,2-Trichloroethane	0.028
Propane	0.042	n-Hexane	0.03	Tetrachloroethylene	0.032
Propylene	0.073	Methacrolein	0.016	2-Hexanone	0
Isobutane	0.02	1,1-Dichloroethane	0.028	Hexanal	0
n-Butane	0.041	Vinyl acetate	0.011	Dibromochloromethane	0.024
Acetylene	0.042	2,4-Dimethylpentane	0.027	1,2-Dibromoethane	0.025
CFC-12	0.032	n-Butyraldehyde	0.019	Chlorobenzene	0.034
Freon-114	0.03	Methylcyclopentane	0.029	Ethylbenzene	0.03
Chloromethane	0.033	cis-1,2-Dichloroethene	0.029	n-Nonane	0.032
1-Butene	0.033	2-Butanone	0.009	m/p-Xylene	0.031
Vinyl chloride	0.03	Ethyl acetate	0.016	o-Xylene	0.029
1,3-Butadiene	0.033	Trichloromethane	0.028	Styrene	0.027
trans-2-Butene	0.029	Tetrahydrofuran	0.001	Tribromomethane	0.028
Acetaldehyde	0.034	2-Methylheptane	0.029	Isopropylbenzene	0.024
cis-2-Butene	0.03	1,1,1-Trichloroethane	0.025	Tetrachloroethane	0.072

Species	MDL	Species	MDL	Species	MDL
Bromomethane	0.031	2,3-Dimethylpentane	0.028	n-Propylbenzene	0.045
Chloroethane	0.032	Cyclohexane	0.03	m-Ethyltoluene	0.042
Isopentane	0.036	3-Methylheptane	0.029	p-Ethyltoluene	0.041
Freon-11	0.031	Carbon tetrachloride	0.025	Decane	0.045
1-Pentene	0.035	Benzene	0.029	1,3,5-Trimethylbenzene	0.042
n-Pentane	0.033	2,2,4-Trimethylpentane	0.028	o-Ethyltoluene	0.04
trans-2-Pentene	0.037	1,2-Dichloroethane	0.028	1,2,4-Trimethylbenzene	0.029
Isoprene	0.033	n-Heptane	0.026	Benzaldehyde	0.028
cis-2-Pentene	0.034	Crotonaldehyde	0.013	1,3-Dichlorobenzene	0.064
Acrolein	0.028	Trichloroethylene	0.031	p-Dichlorobenzene	0.055
Propanal	0.024	Methylcyclohexane	0.031	1,2,3-Trimethylbenzene	0.025
Freon-113	0.032	1,2-Dichloropropane	0.03	Chlorotoluene	0.008
1,1-Dichloroethene	0.038	Methyl methacrylate	0.006	1,3-Diethylbenzene	0.013
2,2-Dimethylbutane	0.034	Pentanal	0.006	p-Diethylbenzene	0.01
Acetone	0.034	1,4-Dioxane	0	Undecane	0.008
Isopropanol	0.014	Bromodichloromethane	0.027	o-Dichlorobenzene	0.052
Carbon disulfide	0.034	2,3,4-Trimethylpentane	0.029	m-Tolualdehyde	0.046

Species	MDL	Species	MDL	Species	MDL
2,3-Dimethylbutane	0.023	2-Methylheptane	0.03	Dodecane	0.002
Dichloromethane	0.032	3-Methylheptane	0.028	1,2,4-Trichlorobenzene	0.013
2-Methylpentane	0.03	trans-1,3-Dichloropropene	0.023	Hexachloro-1,3-butadiene	0.018
Cyclopentane	0.028	Methyl isobutyl ketone	0	Naphthalene	0.005
Methyl tert butyl ether	0.428	Toluene	0.036		
3-Methylpentane	0.026	n-Octane	0.031		

References

Barletta, B., Meinardi, S., Simpson, I. J., Khwaja, H. A., Blake, D. R., and Rowland, F. S.: Mixing ratios of volatile organic compounds (VOCs) in the atmosphere of Karachi, Pakistan, Atmos Environ, 36, 3429-3443, https://doi.org/10.1016/S1352-2310(02)00302-3, 2002.

Li, B., Ho, S. S. H., Gong, S., Ni, J., Li, H., Han, L., Yang, Y., Qi, Y., and Zhao, D.: Characterization of VOCs and their related atmospheric processes in a central Chinese city during severe ozone pollution periods, Atmos. Chem. Phys., 19, 617-638, 10.5194/acp-19-617-2019, 2019.

Mo, Z., Shao, M., Lu, S., Qu, H., Zhou, M., Sun, J., and Gou, B.: Process-specific emission characteristics of volatile organic compounds (VOCs) from petrochemical facilities in the Yangtze River Delta, China, Sci Total Environ, 533, 422-431, https://doi.org/10.1016/j.scitotenv.2015.06.089, 2015.

Russo, R. S., Zhou, Y., White, M. L., Mao, H., Talbot, R., and Sive, B. C.: Multi-year (2004–2008) record of nonmethane hydrocarbons and halocarbons in New England: seasonal variations and regional sources, Atmos. Chem. Phys., 10, 4909-4929, 10.5194/acp-10-4909-2010, 2010.

Shi, J., Deng, H., Bai, Z., Kong, S., Wang, X., Hao, J., Han, X., and Ning, P.: Emission and profile characteristic of volatile organic compounds emitted from coke production, iron smelt, heating station and power plant in Liaoning Province, China, Sci Total Environ, 515-516, 101-108, https://doi.org/10.1016/j.scitotenv.2015.02.034, 2015.

Song, M., Li, X., Yang, S., Yu, X., Zhou, S., Yang, Y., Chen, S., Dong, H., Liao, K., Chen, Q., Lu, K., Zhang, N., Cao, J., Zeng, L., and Zhang, Y.: Spatiotemporal variation, sources, and secondary transformation potential of volatile organic compounds in Xi'an, China, Atmos. Chem. Phys., 21, 4939-4958, 10.5194/acp-21-4939-2021, 2021.

Song, X., Li, X.-B., Yuan, B., He, X., Chen, Y., Wang, S., Huangfu, Y., Peng, Y., Zhang, C., Liu, A., Yang, H., Liu, C., Li, J., and Shao, M.: Elucidating key factors in regulating budgets of ozone and its precursors in atmospheric boundary layer, npj Climate and Atmospheric Science, 7, 262, 10.1038/s41612-024-00818-8, 2024.

Yan, Y., Peng, L., Li, R., Li, Y., Li, L., and Bai, H.: Concentration, ozone formation potential and source analysis of volatile organic compounds (VOCs) in a thermal power station centralized area: A study in Shuozhou, China, Environ Pollut, 223, 295-304, https://doi.org/10.1016/j.envpol.2017.01.026, 2017.

Yuan, B., Shao, M., Lu, S., and Wang, B.: Source profiles of volatile organic compounds associated with solvent use in Beijing, China, Atmos Environ, 44, 1919-1926, https://doi.org/10.1016/j.atmosenv.2010.02.014, 2010.

Zheng, J., Yu, Y., Mo, Z., Zhang, Z., Wang, X., Yin, S., Peng, K., Yang, Y., Feng, X., and Cai, H.: Industrial sector-based volatile organic compound (VOC) source profiles measured in manufacturing facilities in the Pearl River Delta, China, Sci Total Environ, 456-457, 127-136, https://doi.org/10.1016/j.scitotenv.2013.03.055,

2013.